IEEE Access
Multidisciplinary ⋮ Rapid Review ⋮ Open Access Journal

Received 26 March 2024, accepted 6 April 2024, date of publication 12 April 2024, date of current version 22 April 2024.

Digital Object Identifier 10.1109/ACCESS.2024.3387940

RESEARCH ARTICLE

A PSO-SVM-Based Change Detection Algorithm for Remote Sensing Optical Images

BIPIN SHAH[1], AYUSHI GUPTA[1], AND SOURABH PAUL[2]
[1]School of Computer Science and Engineering (SCOPE), Vellore Institute of Technology (VIT), Chennai, Tamil Nadu 600127, India
[2]School of Electronics Engineering (SENSE), Vellore Institute of Technology (VIT), Chennai, Tamil Nadu 600127, India

Corresponding author: Sourabh Paul (sourabh.paul@vit.ac.in)

This work was supported by the Vellore Institute of Technology (VIT), Chennai Campus, Chennai, India.

ABSTRACT Change detection is considered as one of the challenging issues in the field of remote sensing. The multi-temporal images used to detect the changes generally have significant illumination variations which affect the performance of a change detection method. To address this issue, a machine learning (ML)-based change detection algorithm is proposed for the remote sensing optical images. The proposed method is a combination of Support Vector Machines (SVM) and Particle Swarm Optimization (PSO). In this method, the PSO is utilized in a novel way to provide the optimized feature vectors. These feature vectors are used in SVM to accurately determine the changed and unchanged pixels. The proposed method is very effective in identifying the changes in remote sensing optical images having significant illumination variations. It can give comparatively higher correct classification (PCC) values, and lower false alarm (PFA) as well as total error (PTE) values than the state-of-the-art methods. Experiments on six pairs of Landsat images demonstrate the effectiveness of the proposed method.

INDEX TERMS Machine learning (ML), particle swarm optimization (PSO), support vector machines (SVM).

I. INTRODUCTION

Change detection is the systematic identification and analysis of alterations in data or physical phenomena over time. This process holds profound significance across diverse fields, from environmental monitoring and remote sensing to healthcare, finance, and the social sciences. By recognizing and quantifying changes in various contexts, change detection enables us to make informed decisions, monitor trends, and respond to evolving circumstances effectively. Change detection plays a crucial role in the domain of remote sensing. By comparing spectral and spatial characteristics in remote sensing images, the alterations in land cover, vegetation, and urban development are identified. This capability is invaluable for applications such as environmental monitoring, urban planning, disaster management, and agriculture. The change detection process can be broadly classified into unsupervised, and supervised methods.

The associate editor coordinating the review of this manuscript and approving it for publication was Manuel Rosa-Zurera.

Unsupervised change detection techniques in the realm of remote sensing have garnered significant attention due to their ability to uncover changes on the Earth's surface without relying on ground truth data [1], [2], [3], [4], [5], [6], [7], [8], [9], [10], [11], [12], [13], [14], [15], [16], [17], [18], [19], [20], [21], [22], [23], [24], [25], [26]. These techniques encompass various approaches, each offering unique insights into the detection of alterations. In [1], an innovative methodology was proposed for change detection by analyzing pairs of cross-sharpened images which effectively reduced the overestimation of changed areas. Gupta et al. [2] implemented the Local Binary Similarity Pattern (LBSP) technique to identify changes in optical satellite images. In this method, a novel threshold technique based on the Hamming distance is proposed to create binary feature vectors and binary change maps. Also, in [3], Gupta et al. used a local neighborhood information (LNI) to construct the feature vector. This method involves processing of two images by partitioning them into overlapping blocks, concatenating corresponding blocks from the images, and applying Otsu's thresholding method. Celik et al. [4] adopted the

mean square error (MSE) between different images and employed genetic algorithms (GA) to identify changes at the lowest possible cost. This method achieves 1.82% total error rate and, hence, 98.18% correct detection rate. In contrast, Zhang et al. [5] introduced the concept of ''spectrum trend'', which utilizes spectral values within specific geographic areas. Although this method was effective, it faces challenges in selecting appropriate image window sizes and aims to enhance local spectrum-trend similarity (LSTS). Also, in [6], Celik introduced the S-levels undecimated discrete wavelet transform (UDWT) in unsupervised change detection, coupled with k-means clustering for generating change detection maps. This method demonstrates robustness against noise. Luo et al. [7] introduced a soft-change detection technique, treating it as a transparency computation problem and optimizing an objective function using Bayesian matting. Kalinicheva et al. [8] employed neural network autoencoders (AEs) to generate bitemporal change masks, facilitating comprehensive change analysis. Principal component analysis (PCA) and k-means clustering were explored in [9]. In this method, the difference image is divided into non-overlapping blocks for change identification. In addition, the multiscale structure of the dual-tree complex wavelet transform (DT-CWT) was utilized in [10], offering an unsupervised change-detection method based on DT-CWT. Meanwhile, in [11], Generative Adversarial Networks (GANs) focused on generating co-registered images to facilitate change identification for image quality and clip position improvements. This method got the F1 score as 0.7692. The paper [12] presents an innovative approach to oil spill monitoring in optical remote sensing images, utilizing multitemporal change detection techniques for unsupervised, semiautomatic, and efficient detection. Zhan et.al [13] introduced an unsupervised change detection method for heterogeneous synthetic aperture radar (SAR) and optical images, utilizing a logarithmic transformation feature learning framework to align statistical distribution properties. In [14], Sibling Regression for Optical Change detection (SiROC) method designed for change detection in optical satellite images. SiROC gains about 12 percentage points (p.p.) in specificity, 7 p.p. in sensitivity, 12 p.p. in precision. In [15], a Deep Change Vector Analysis (DCVA) framework was presented for change detection in very high spatial resolution (VHR) multitemporal optical satellite images. Yetgin et al. [16] proposed an invisible transform detection method for multi-temporal satellite images using Gaussian mixture model (GMM), mean square descent, and k-means clustering. The authors in [17] proposed a method for multitemporal satellite images, utilizing a novel detail-enhancing algorithm. This method involves combining the coefficients of the directional sub bands to extract the main points which are then injected into the base image to create a contrast-enhanced image. The method receives a total error rate of 7.59%. In [18], a transform detection method for heterogeneous multi-temporal satellite images based on unsupervised images was used. In [19], a new unsupervised transformation was presented for recognizing heterogeneous remote sensing image pairs. This method uses parameter estimation parameters with a two-norm function model in multiple solutions, which improves the estimation quality. The method in [20] introduced a new parameter mapping strategy for transformation in heterogeneous dual-time satellite image detection. In [21], Radoi et al. incorporated Hamming distance and binary descriptors to train a supervised model. The utilization of vector quantization streamlined the management of change-related data, facilitating accessibility and improved model performance. Celik et al. [22] proposed an invisible transform detection method for satellite images. The method yields a 0.34% total erroneous decision rate. Prendes et.al [23] proposed a novel approach for measuring similarity between remote sensing images from heterogeneous sensors, using manifold learning to infer sensor properties and noise models. In [24], a spatiotemporal fusion change detection (STFCD) algorithm was used for flood extent monitoring using multisource heterogeneous satellite image time series (MSH-SITS). In [25], a parallel binary particle swarm optimization (PBPSO) was used to create a binary change-detection mask using particle swarm optimization (PSO). The method obtains the least overall error of 0.67%. In [26], an unsupervised change detection technique was presented using the scale-invariant feature transform (SIFT)-flow algorithm. This method receives a F1 score of 81.65%.

Supervised change detection techniques use labeled data to enhance the accuracy and efficiency of change identification. These techniques can be further classified as machine learning (ML)-based and deep learning-based methods. A variety of ML-based change detection methods are reported in [27], [28], [29], [30], [31], and [32]. The change detection algorithm proposed in [27] was based on the use of a Random Forest (RF) algorithm for land use and land cover classification. This method achieved an overall accuracy of 96% for landcover change detection. In [28], the quantile regression and copula theory were used to detect the changes. In [29], the performance of the firefly support vector machines (FF-SVM) algorithm was improved by using various filtering techniques including F-score, Joint Mutual Information (JMI), Maximum Relevance Minimum Redundancy (mRMR), and Double Input Symmetrical Relevance (DISR). Additionally, various methods have been employed to accelerate Support Vector Machines (SVM) for change detection in satellite images. One notable approach proposed by Habib et al. in [30], focuses on reducing the number of support vectors. Longbotham et al. [31] presented a predictive model based on digital progress data that provided insight into the field of flood detection. In [32], a methodology was introduced for the multitemporal and contextual classification of georeferenced optical remote sensing images employing Conditional Random Fields (CRFs).

In [33], [34], [35], [36], [37], [38], [39], and [40], different deep learning-based methods are proposed for change detection. In [33], Li et al. addressed concerns related to change detection in image boundaries and varying viewing angles

by introducing a Siamese change detection network within a multitask learning framework. In [34], an efficient satellite image change detection network DifUnet++ was presented. This model incorporates a pyramid of two input images and employs advanced up-sampling techniques to enhance the granularity of change detection, further advancing the state-of-the-art in the field. Jing et al. [35] proposed a novel approach which combined multi-scale Simple Linear Iterative Clustering-Convolutional Neural Network (SLICCNN) and Stacked Convolutional Auto-Encoder (SCAE) features. Basavaraju et al. [36] introduced the Urban Change Detection Network (UCDNet) model for urban change detection. Chouhan et al. [37] introduced Difference Image Reconstruction Enhanced Multiresolution Network (DRMNet), a multivariate learning model designed for transformation in satellite imagery. In [38], the authors introduced an end-to-end deep neural network called as Difference-Enhancement Triplet Network (DETNet) for multivariate detection. In [39], a model was introduced which explored the challenges and opportunities associated with high spatial resolution optical satellite imagery for monitoring land cover changes. It presents an innovative change detection method grounded in neural networks, significantly mitigating human intervention, and achieving a notable 2-3 times reduction in classification errors compared to conventional post classification approaches. In [40], an intriguing avenue was presented for change detection through Canonical Correlation Analysis (CCA). This approach tends to perform optimally in scenarios where changes exhibit a smooth and gradual spread, showcasing the adaptability of reinforcement learning in addressing change detection challenges.

Although a variety of methods have been proposed in recent years to detect changes in optical images, most of them are unsupervised methods. Generally, the supervised methods give better accuracy than the unsupervised methods. These are more suitable for handling images with nonlinear intensity differences. In the literature, several deep learning methods can be found which are used to detect the changes in remote sensing images. However, it is a well-known fact that the deep learning methods require significantly higher computational time to train the model. In addition, these methods also need a large amount of labeled data in training to provide optimal performance. But, a large amount of labeled data generation from the remote sensing images is a critical task. In order to address these issues, we have proposed a ML-based method that combines SVM and PSO. The main advantages of using a ML method are as follows: (i) it takes less computational time in training compared to the deep learning methods, (ii) it does not require a large amount of labeled data to train the model and (iii) the inclusion of the proposed optimization technique improves the detection performance.

The novelties of the proposed method are as follows:

1) An ML-based change detection algorithm is proposed to work automatically. The proposed method uses an improved version of the SVM algorithm to automatically detect the changed and unchanged pixels between input optical images.

2) The PSO is utilized along with the SVM in a novel way to provide the optimized feature vectors. These optimized feature vectors are used to train an SVM model which provides better accuracy in identifying the changed and unchanged pixels.

II. PROPOSED METHODOLOGY

A. SVM

SVM is a supervised ML algorithm that originated in the computer science and statistics field. It has found widespread applications across various domains due to its effectiveness in classification and regression tasks. The algorithm's development was motivated by the need for a robust method for pattern recognition and classification. It is primarily used for classification tasks, where it categorizes data points into different classes based on their features. It can also be used for regression, where it predicts a continuous output variable based on input features. SVM was originally conceived as a solution to the problem of finding a hyperplane that best separates two classes of data in a high-dimensional space. The decision function f is defined as follows:

$$f(x) = w.x + b \tag{1}$$

$$w = \sum_{i=1}^{N} \alpha_i y_i x_i \tag{2}$$

where, x is the input feature vector, w is a vector perpendicular to a hyperplane that separates two classes, b is an offset value, α is a Lagrange multiplier, and y denotes the class label. Its origins lie in the quest for a robust and efficient method for pattern recognition and classification in complex data sets.

Although the SVM algorithm is computationally intensive, still it can result in unsatisfactory performance if the input feature vectors are not appropriately optimized. Therefore, it is imperative to have techniques in place to expedite the SVM classification process [41]. In [30], a novel hybrid classification model was employed with SVM to offer a promising solution for addressing gene selection and cancer classification challenges. Motivated by this fact, we have used the PSO algorithm to optimize the feature vector before applying the features in SVM to determine the changed and unchanged pixels.

B. PSO

PSO is an optimization method developed by the collective behaviors observed in birds flocking or fish schooling. It simulates the movement of particles within a search space to discover the best possible solution to a problem. The particle with the best-known position (global best) at the end of the optimization process represents the optimal solution to the problem. It has a wide range of applications in ML, Bioinformatics, Telecommunication, etc. Its effectiveness lies in its ability to explore a search space efficiently and find near-optimal solutions for complex optimization problems.

In PSO, the velocity and position of each particle are updated depending on the search experience of the whole swarm and the individual particle. The following equations are used for updating the velocity (V) and the position (X) of the particles:

$$V_i(t+1) = \omega V_i(t) + r_1 c_1 \left[Pbest_i - X_i(t)\right] + r_2 c_2 \left[gbest(t+1) - X_i(t)\right] \quad (3)$$

$$X_i(t+1) = X_i(t) + V_i(t+1) \quad (4)$$

where t denotes the iteration index, ω is the inertia weight, c_1 and c_2 are learning factors, r_1 and r_2 are random numbers that are uniformly distributed in [0,1], V_i is the velocity of the i^{th} particle, $Pbest_i$ is the personal best position of the i^{th} particle, and $gbest$ is the global best position of the swarm.

C. PROPOSED PSO-SVM-BASED TRAINING

The proposed PSO-SVM algorithm combines the PSO and the SVM to provide better accuracy in change detection. In this method, the PSO is used to find the best particle. Then, this particle is used to train the SVM to improve the classification accuracy. Fig. 1 presents the flow chart of the proposed method.

Let I_1 and I_2 be the two co-registered optical images of size n x m pixels that are captured at different times. These are divided into 5×5 pixels overlapping blocks. Therefore, a block of size 5×5 pixels is considered around each pixel of the image, and every pixel corresponds to the center of the block. Then, two difference vectors D_1 and D_2 are constructed for each pixel. The first vector D_1 is calculated by taking the absolute difference between the center pixel and 25 pixels of the corresponding block of I_1. Similarly, D_2 is calculated by taking the absolute difference between the center pixel of the block of I_1 and 25 pixels of the corresponding block of the image I_2. Both vectors are of size 25×1.

$$D_1(a,b) = \{x_1, x_2, x_3, \ldots\ldots, x_{25}\} \quad (5)$$

$$D_2(a,b) = \{y_1, y_2, y_3, \ldots\ldots, y_{25}\} \quad (6)$$

where D_1 denotes the absolute difference vector created by the center pixel of I_1 and its corresponding block. D_2 is the absolute difference vector created by the center pixel of I_1 and its corresponding block of I_2. $(a,\ b)$ represents the position of the pixel in the image, where $a = \{1, 2, \ldots, n\}$ and $b = \{1, 2, \ldots, n\}$. These vectors D_1 and D_2 are concatenated to construct the feature vector D of size 50×1.

$$D(a,b) = \{x_1, x_2, x_3, \ldots\ldots, x_{25}, y_1, y_2, y_3, \ldots\ldots, y_{25}\} \quad (7)$$

The same procedure is followed to create feature vectors for each pixel of the images.

Now, $2N$ feature vectors are selected randomly and their combination is considered as a particle in our proposed method. Out of these $2N$ feature vectors, N vectors are taken from changed positions, and the remaining N vectors are from the unchanged positions. This procedure is followed s times

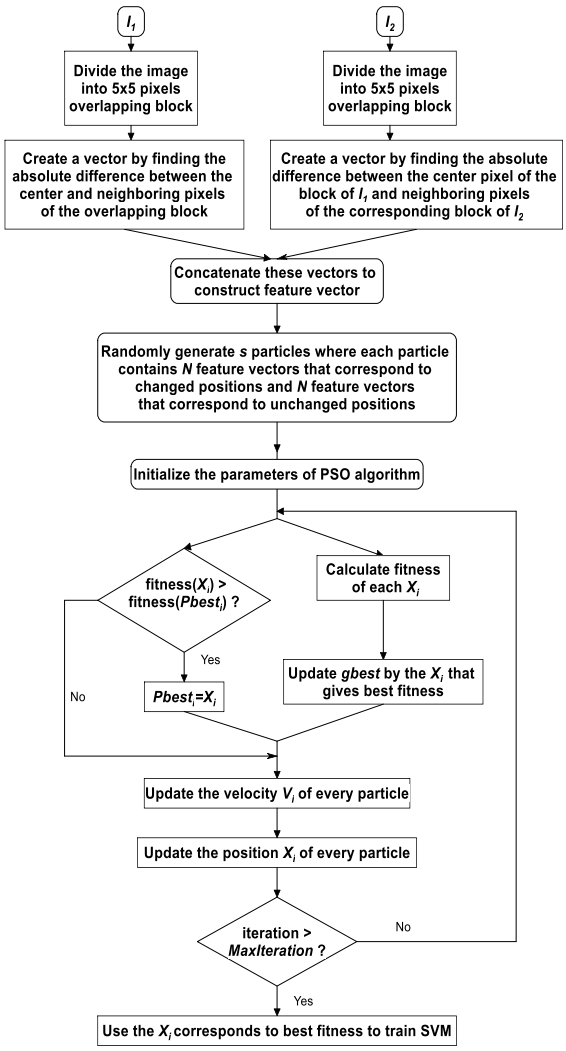

FIGURE 1. Flow chart of the proposed methodology.

to generate s different particles. The velocity and position of these particles are updated by using equations (3) and (4), respectively. In equation (3), the $gbest$ and $Pbest$ values are updated by considering a validation set of size M, which contains feature vectors of changed and unchanged pixels. If the fitness of the current X_i is more than the current $Pbest_i$, then $Pbest_i$ is updated by this X_i. Otherwise, $Pbest_i$ remains unchanged. The fitness of each X_i in the current iteration is calculated, and the best fitness value is found. If this value is greater than the current $gbest$, then the $gbest$ is updated by that corresponding X_i that gives the best fitness. Here, the fitness is calculated by applying the corresponding set of feature vectors in an SVM model and then, that model is used to predict the label of features in the validation set. In our proposed method, fitness is defined as the ratio of the number of True Positive (TP) of this prediction to the number of samples in the validation set.

Equations (3) and (4) are updated until they reach the maximum iteration ($MaxIteration$). Then, the fitness values of all the optimized particles are calculated, which are obtained

Algorithm 1 PSO-SVM-Based Training

Input:

- s: Number of particles in the swarm
- X_i: Position of the i^{th} particle
- Vi: Velocity of the i^{th} particle
- *MaxIteration*: Maximum iterations
- *Valid_Set*: Validation set

Output: SVM model trained with best particle

Algorithm:

1) Initialize PSO parameters
2) **for** $t = 1$ to *MaxIteration* **do**
3) Evaluate the *fitness* of each particle using *Valid_Set*
4) **for** $i = 1$ to s **do**
5) **if** $fitness(X_i) > fitness(gbest)$ **do**
6) $gbest = X_i$
7) **end if**
8) **end for**
9) **for** $i = 1$ to s **do**
10) **if** $fitness(Pbest_i) > fitness(X_i)$ **do**
11) $Pbest_i = X_i$
12) **end if**
13) **end for**
14) **for** $i = 1$ to s **do**
15) Update V_i using equation (3)
16) Update X_i using equation (4)
17) **end for**
18) **end for**
19) Find the particle X_b that gives the best fitness among all X_i
20) Train the SVM with X_b

after the *MaxIteration* iteration. Finally, the particle with the best fitness value is used to train the SVM. This trained SVM model is used to predict the label of feature vectors in the test set which contains the feature vectors of changed and unchanged positions. The steps followed in the proposed method are provided in Algorithm 1.

III. EXPERIMENTAL RESULTS

The effectiveness of the proposed method is evaluated using six optical remote sensing datasets [42]. The Landsat TM (Thematic Mapper) Collection 2 (C2) Level 1 (L1) and 2 (L2) data, specifically Band 5 is used for the experiments.

A. DATASET DESCRIPTION

The first dataset comprises two images captured by Landsat TM C2 L2 covering an area of the Shahjad reservoir, situated approximately 3 kilometers from Lalitpur, Uttar Pradesh. The first image was captured on April 11, 1998, while the second image was obtained on April 9, 2009. These images serve as valuable resources for analyzing land cover changes and environmental dynamics in the region over eleven-year period and have a size of 200 × 200 pixels. These are shown in Fig. 2(a) and (b), and the ground truth is in Fig. 2(c), which shows the changed and unchanged pixels.

The second pair of images consists of two images of size 200 × 200 pixels as shown in Fig. 3(a) and (b). These were acquired by Landsat TM C2 L2 on December 12, 1989, and on May 12, 2010. This data set covers the Ghod Dam in Wadgaon Shindodi, Maharashtra which represents

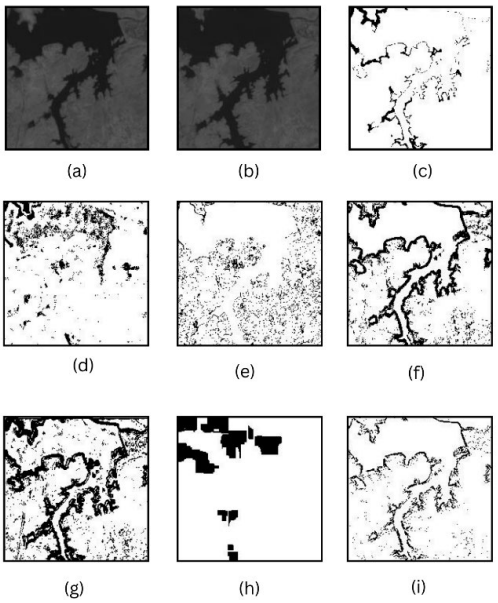

FIGURE 2. Results of Dataset I (a), (b) Landsat TM C2 L2 and 5 of Shahjad reservoir, Uttar Pradesh (c) Ground Truth (d) LBSP [2] (e) LNI [3] (f) SVM (g) RF [27] (h) SIFT Flow [26] (i) Proposed.

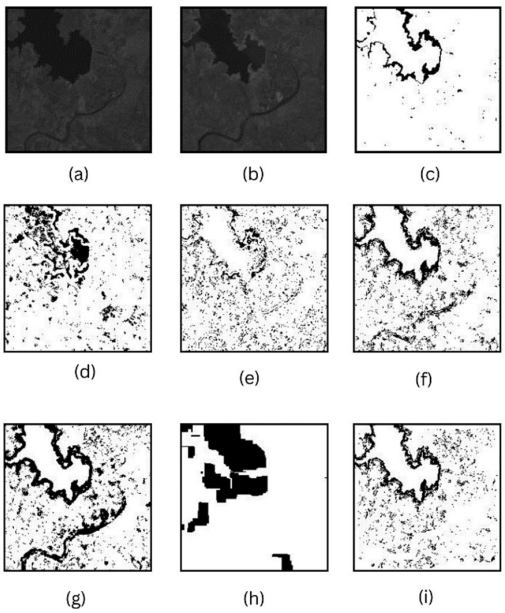

FIGURE 3. Results of Dataset II (a), (b) Landsat TM C2 L2 Band 5 of Ghod Dam, Maharashtra (c) Ground Truth (d) LBSP [2] (e) LNI [3] (f) SVM (g) RF [27] (h) SIFT Flow [26] (i) Proposed.

the changes in that region. Fig. (c) shows the corresponding ground truth image.

The third dataset is captured by Landsat TM C2 L2 images over an area of Pench reservoir, Navegaon, Maharashtra. The images of this set were captured on May 21, 1992 and April 21, 2010 and have a size of 200 × 200 pixels. The images of this data set and the corresponding ground truth image are shown in Fig. 4(a), 4(b), and 4(c), respectively. This dataset represents the changes in reservoir area.

The fourth dataset as shown in Fig. 5(a) and (b) consists of two images of size 200 × 200 pixels. These were acquired

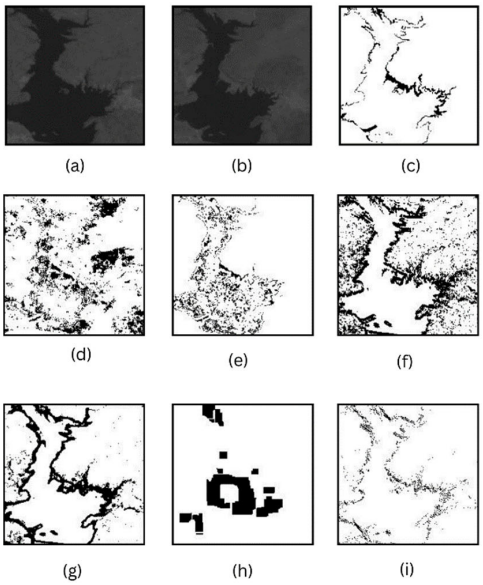

FIGURE 4. Results of Dataset III (a), (b) Landsat TM C2 L2 Band 5 of Pench reservoir, Maharashtra (c) Ground Truth (d) LBSP [2] (e) LNI [3] (f) SVM (g) RF [27] (h) SIFT Flow [26] (i) Proposed.

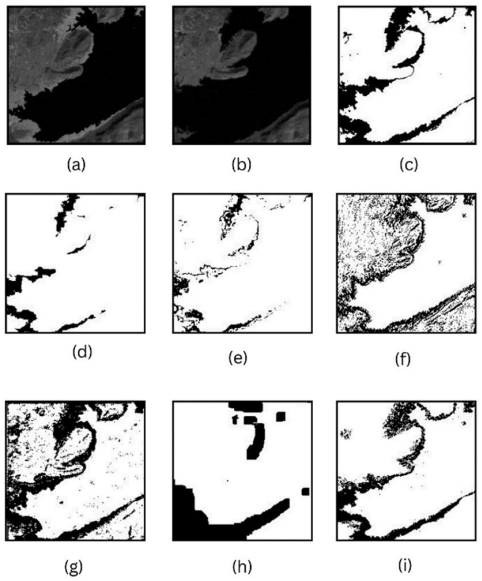

FIGURE 5. Results of Dataset IV (a), (b) Landsat TM C2 L1 Band 5 of Yeleru reservoir, Andhra Pradesh (c) Ground Truth (d) LBSP [2] (e) LNI [3] (f) SVM (g) RF [27] (h) SIFT Flow [26] (i) Proposed.

by Landsat TM C2 L1 covering an area of Yeleru reservoir, Andhra Pradesh. The first image of this set was captured on December 9, 2003, while the second image on January 13, 2013. This dataset represents the increased area of reservoir. The corresponding ground truth image is shown in 5(c).

The fifth dataset contains two Landsat TM C2 L1 images of Devhari Chikhli, Maharashtra. The initial image was taken on May 6, 1993, and the subsequent one on May 5, 2010. This dataset represents the changes in water bodies in Maharashtra. These images have a size of 200 × 200 pixels. Fig. 6(a), 6(b), and 6(c) show these images and the corresponding ground truth images, respectively.

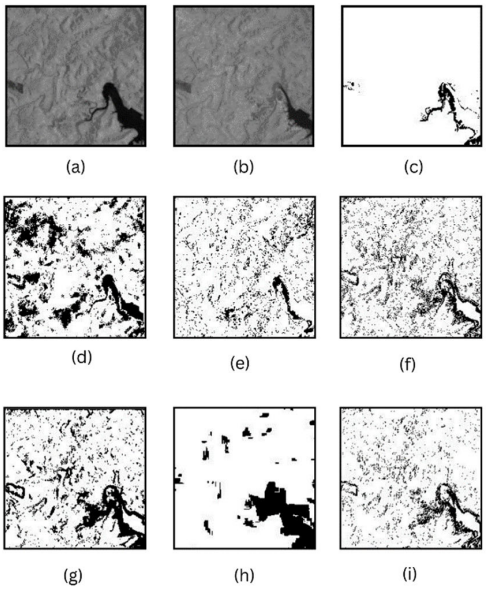

FIGURE 6. Results of Dataset V (a), (b) Landsat TM C2 L1 Band 5 of Devhari Chikhli, Maharashtra (c) Ground Truth (d) LBSP [2] (e) LNI [3] (f) SVM (g) RF [27] (h) SIFT Flow [26] (i) Proposed.

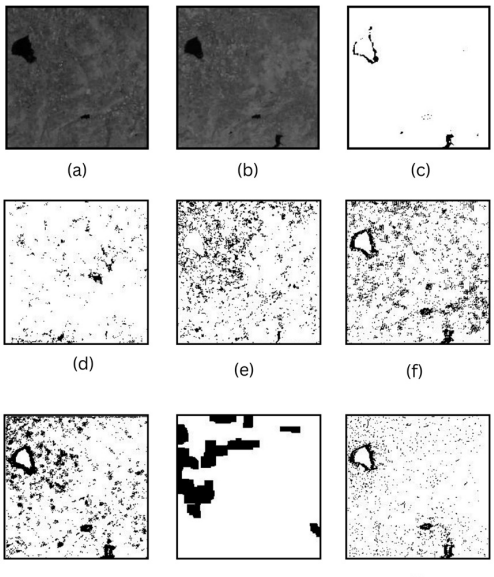

FIGURE 7. Results of dataset VI (a), (b) Landsat TM C2 L1 Band 5 of Daunapur Dam, Maharashtra (c) Ground Truth (d) LBSP [2] (e) LNI [3] (f) SVM (g) RF [27] (h) SIFT Flow [26] (i) Proposed.

The last dataset covers an area of Daunapur Dam, Maharashtra and the images of this set were captured by Landsat TM C2 L1 on October 14, 1996 and November 8, 2011. They have a size of 200 × 200 pixels. The images of this data set are shown in Fig. 7(a) and (b), and Fig. (c) shows the corresponding ground truth image. This dataset represents the changes in Daunapur Dam region.

B. QUANTITATIVE PARAMETERS

The following quantitative assessments parameters are computed to show the performance of the proposed method:

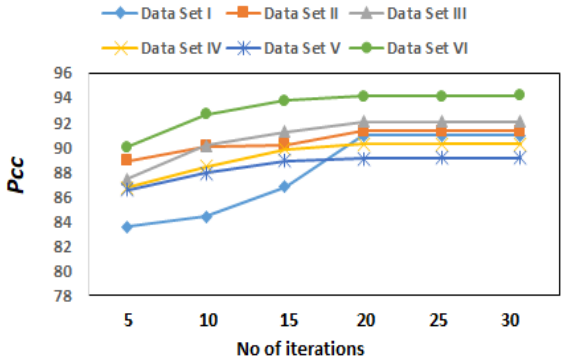

FIGURE 8. P_{CC} values for different numbers of iterations in PSO-SVM algorithm.

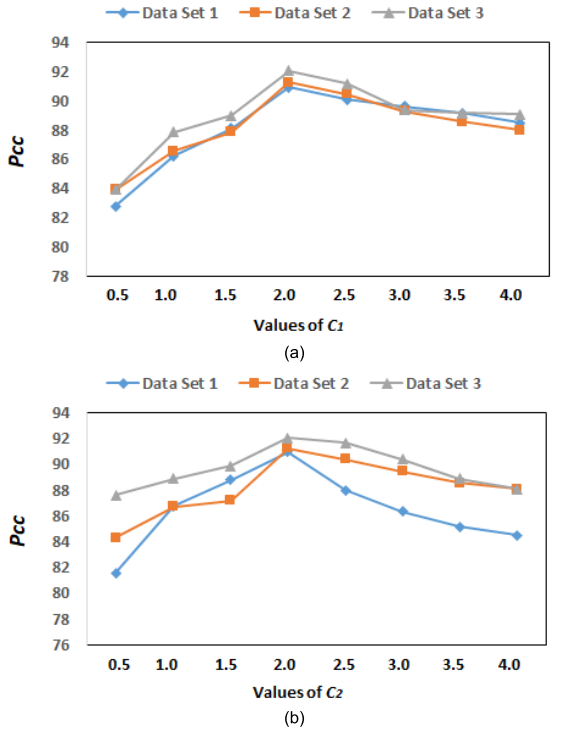

FIGURE 9. (a) Effects of c_1 on P_{CC} (b) Effects of c_2 on P_{CC}.

1. Correct Classification (P_{CC})

$$P_{CC} = \left(\frac{TP + TN}{N_0 + N_1}\right) 100 \tag{8}$$

2. False Alarms (P_{FA})

$$P_{FA} = \frac{FP}{N_1} \tag{9}$$

3. Total Error (P_{TE})

$$P_{TE} = \left(\frac{FP + FN}{N_0 + N_1}\right) 100 \tag{10}$$

where TP is the total number of changed pixels that were correctly identified as changed, TN is the total number of unchanged pixels that were correctly identified as unchanged, N_0 is the total number of changed pixels, N_1 is the total number of unchanged pixels, FP is total number of unchanged pixels that were incorrectly identified as changed and FN is the total number of changed pixels that were incorrectly identified as unchanged.

TABLE 1. Performance measures in terms of P_{CC}, P_{FA} and P_{TE}.

Dataset	METHOD	P_{CC}	P_{FA}	P_{TE}
Dataset I	LBSP	87.65	0.10	12.3
	LNI	87.88	0.09	12.12
	SVM	83.05	0.16	16.95
	RF	76.35	0.24	23.65
	SIFT Flow	85.63	0.11	14.37
	PROPOSED	**90.96**	**0.06**	**9.04**
Dataset II	LBSP	87.18	0.11	12.82
	LNI	88.89	0.09	11.11
	SVM	85.88	0.14	14.12
	RF	81.58	0.18	18.42
	SIFT Flow	83.86	0.16	16.14
	PROPOSED	**91.28**	**0.08**	**8.72**
Dataset III	LBSP	80.54	0.16	19.46
	LNI	88.78	0.08	11.22
	SVM	83.13	0.19	16.87
	RF	87.41	0.13	12.59
	SIFT Flow	87.56	0.10	12.44
	PROPOSED	**92.08**	**0.05**	**7.92**
Dataset IV	LBSP	88.94	0.14	11.06
	LNI	89.13	0.08	10.87
	SVM	82.52	0.13	17.48
	RF	83.35	0.16	16.65
	SIFT Flow	83.02	0.12	16.98
	PROPOSED	**90.25**	**0.05**	**9.75**
Dataset V	LBSP	77.23	0.22	22.77
	LNI	87.98	0.10	12.02
	SVM	85.04	0.14	14.96
	RF	83.31	0.16	16.69
	SIFT Flow	88.04	0.11	11.96
	PROPOSED	**89.09**	**0.09**	**10.91**
Dataset VI	LBSP	87.98	0.07	12.02
	LNI	88.38	0.11	11.62
	SVM	84.55	0.13	15.45
	RF	86.01	0.14	13.99
	SIFT Flow	85.68	0.14	14.32
	PROPOSED	**94.15**	**0.05**	**5.85**

C. PARAMETER SETTING

In our proposed PSO-SVM algorithm, the values of *MaxIteration*, c_1, and c_2 are determined by analyzing the experimental results of the selected data sets. Fig. 8 shows that, initially, the value of P_{CC} increases with the increase in the number of iterations. However, after 20 iterations, there is no improvement in the P_{CC} values. Therefore, *MaxIteration* is set to 20. Fig. 9 shows the effects of c_1 and c_2 on P_{CC} values. It can be observed that the maximum value of P_{CC} is obtained when the values of c_1 and c_2 are considered as 2. Therefore, the values of c_1 and c_2 are set to 2. If too many particles are considered in the swarm, then it takes significant computational time in training. On the other hand, a smaller number of particles may not give the optimized results. Considering these facts, the value of s is set to 10. The value of ω is considered as 0.5. In addition, the value of N is set to 150. A very small value of N results in insufficient features, whereas a very large value of N takes significant computational time in the training phase.

D. RESULT ANALYSIS

The proposed scheme is compared with the five state-of-the-art methods such as LBSP [2], LNI [3], SVM, RF [27], and SIFT Flow [26] to demonstrate its efficacy. Table 1 presents the quantitative results of the LBSP [2], LNI [3], SVM, RF [27], SIFT Flow [26] and proposed method. From this table, it can be observed that the LNI [3] method obtains comparatively better P_{CC}, P_{FA}, and P_{TE} values than the LBSP [2], SVM and RF [27] methods for all six datasets. Moreover, it gives better results than the SIFT Flow [26] for datasets I, II, III, IV, and V. However, the SIFT Flow [26] outperforms the LNI [3] for dataset V. The LBSP [2] method gives better performance than the SVM, RF [27] and SIFT Flow [26] methods for datasets I, II, IV and VI. The SVM obtains better results than the LBSP [2], RF [27] and SIFT Flow [26] methods for dataset III. However, the best results are obtained by the proposed method in all six cases.

The proposed method achieves a P_{CC} value of 90.96%, P_{FA} of 0.06, and P_{TE} of 17.07% for dataset I. The proposed method outperforms the compared methods for dataset II with a P_{CC} of 91.28%, P_{FA} of 0.08, and P_{TE} of 8.78%. For dataset III, it obtains a P_{CC} value of 92.08%, P_{FA} of 0.05 and the P_{TE} of 7.92%. For dataset IV, P_{CC} is 90.25%, P_{FA} is 0.05 and P_{TE} is 9.75%. For dataset V, the obtained P_{CC}, P_{FA}, P_{TE} values are 89.09%, 0.09, and 10.91%, respectively. Moreover, for dataset VI, P_{CC} is 94.15%, P_{FA} is 0.05 and P_{TE} is 5.85%. Fig. 2, Fig. 3, Fig.4, Fig. 5, Fig. 6, and Fig. 7 show the visual results obtained by different methods for dataset I, data set II, dataset III, dataset IV, dataset V, and dataset VI, respectively. From these visual results, it is obvious that the changed map obtained by the proposed method is more accurate than the LBSP [2], LNI [3], SVM, RF [27] and the SIFT Flow [26] methods.

The SVM and RF fall short in achieving high accuracy because these methods do not use optimized features for model training, unlike the technique proposed in this paper. Additionally, the LBSP, LNI and SIFT Flow construct change map using thresholding criteria. This technique fails to correctly represent the changed and unchanged positions in many cases where the intensity variations and noise effects are significant. As a result, these methods do not give better performance than the proposed approach.

IV. CONCLUSION

In this letter, a novel supervised method is introduced that combines PSO with the SVM to enhance accuracy in change detection. The integration of PSO with the SVM facilitates the automatic selection of optimal features for training the model, which provides significant improvement in accuracy. The experiments have demonstrated the effectiveness of the proposed method in change detection tasks. In summary, the key advantages of the proposed algorithm are as follows:

1) Automation: Our method utilized the power of ML to automate the feature selection process, reducing the need for manual intervention, and making the process of change detection more efficient and organized.

2) Enhanced Accuracy: The experimental results establish that our approach consistently delivers superior accuracy in change detection tasks, making it a valuable tool for a wide range of applications.

Through this research, we have contributed to the advancement of change detection techniques, offering a robust and efficient approach that holds promise for various domains where an accurate change detection is a key factor.

REFERENCES

[1] B. Wang, S. Choi, Y. Byun, S. Lee, and J. Choi, "Object-based change detection of very high resolution satellite imagery using the cross-sharpening of multitemporal data," *IEEE Geosci. Remote Sens. Lett.*, vol. 12, no. 5, pp. 1151–1155, May 2015.

[2] N. Gupta, G. V. Pillai, and S. Ari, "Change detection in optical satellite images based on local binary similarity pattern technique," *IEEE Geosci. Remote Sens. Lett.*, vol. 15, no. 3, pp. 389–393, Mar. 2018.

[3] N. Gupta, G. V. Pillai, and S. Ari, "Change detection in landsat images based on local neighbourhood information," *IET Image Process.*, vol. 12, no. 11, pp. 2051–2058, Nov. 2018.

[4] T. Celik, "Change detection in satellite images using a genetic algorithm approach," *IEEE Geosci. Remote Sens. Lett.*, vol. 7, no. 2, pp. 386–390, Apr. 2010.

[5] P. Zhang, Z. Lv, and W. Shi, "Local spectrum-trend similarity approach for detecting land-cover change by using SPOT-5 satellite images," *IEEE Geosci. Remote Sens. Lett.*, vol. 11, no. 4, pp. 738–742, Apr. 2014.

[6] T. Celik, "Multiscale change detection in multitemporal satellite images," *IEEE Geosci. Remote Sens. Lett.*, vol. 6, no. 4, pp. 820–824, Oct. 2009.

[7] W. Luo and H. Li, "Soft-change detection in optical satellite images," *IEEE Geosci. Remote Sens. Lett.*, vol. 8, no. 5, pp. 879–883, Sep. 2011.

[8] E. Kalinicheva, D. Ienco, J. Sublime, and M. Trocan, "Unsupervised change detection analysis in satellite image time series using deep learning combined with graph-based approaches," *IEEE J. Sel. Topics Appl. Earth Observ. Remote Sens.*, vol. 13, pp. 1450–1466, 2020.

[9] T. Celik, "Unsupervised change detection in satellite images using principal component analysis and *k*-means clustering," *IEEE Geosci. Remote Sens. Lett.*, vol. 6, no. 4, pp. 772–776, Oct. 2009.

[10] T. Celik and K.-K. Ma, "Unsupervised change detection for satellite images using dual-tree complex wavelet transform," *IEEE Trans. Geosci. Remote Sens.*, vol. 48, no. 3, pp. 1199–1210, Mar. 2010.

[11] C. Ren, X. Wang, J. Gao, X. Zhou, and H. Chen, "Unsupervised change detection in satellite images with generative adversarial network," *IEEE Trans. Geosci. Remote Sens.*, vol. 59, no. 12, pp. 10047–10061, Dec. 2021.

[12] S. Liu, M. Chi, Y. Zou, A. Samat, J. A. Benediktsson, and A. Plaza, "Oil spill detection via multitemporal optical remote sensing images: A change detection perspective," *IEEE Geosci. Remote Sens. Lett.*, vol. 14, no. 3, pp. 324–328, Mar. 2017.

[13] T. Zhan, M. Gong, X. Jiang, and S. Li, "Log-based transformation feature learning for change detection in heterogeneous images," *IEEE Geosci. Remote Sens. Lett.*, vol. 15, no. 9, pp. 1352–1356, Sep. 2018.

[14] L. Kondmann, A. Toker, S. Saha, B. Schölkopf, L. Leal-Taixé, and X. X. Zhu, "Spatial context awareness for unsupervised change detection in optical satellite images," *IEEE Trans. Geosci. Remote Sens.*, vol. 60, 2022, Art. no. 5614615.

[15] S. Saha, F. Bovolo, and L. Bruzzone, "Unsupervised deep change vector analysis for multiple-change detection in VHR images," *IEEE Trans. Geosci. Remote Sens.*, vol. 57, no. 6, pp. 3677–3693, Jun. 2019.

[16] Z. Yetgin, "Unsupervised change detection of satellite images using local gradual descent," *IEEE Trans. Geosci. Remote Sens.*, vol. 50, no. 5, pp. 1919–1929, May 2012.

[17] S. Li, L. Fang, and H. Yin, "Multitemporal image change detection using a detail-enhancing approach with nonsubsampled contourlet transform," *IEEE Geosci. Remote Sens. Lett.*, vol. 9, no. 5, pp. 836–840, Sep. 2012.

[18] Y. Sun, L. Lei, D. Guan, M. Li, and G. Kuang, "Sparse-constrained adaptive structure consistency-based unsupervised image regression for heterogeneous remote-sensing change detection," *IEEE Trans. Geosci. Remote Sens.*, vol. 60, 2022, Art. no. 4405814.

[19] R. Touati, M. Mignotte, and M. Dahmane, "A reliable mixed-norm-based multiresolution change detector in heterogeneous remote sensing images," *IEEE J. Sel. Topics Appl. Earth Observ. Remote Sens.*, vol. 12, no. 9, pp. 3588–3601, Sep. 2019.
[20] M. Mignotte, "A fractal projection and Markovian segmentation-based approach for multimodal change detection," *IEEE Trans. Geosci. Remote Sens.*, vol. 58, no. 11, pp. 8046–8058, Nov. 2020.
[21] A. Radoi and M. Datcu, "Automatic change analysis in satellite images using binary descriptors and Lloyd–Max quantization," *IEEE Geosci. Remote Sens. Lett.*, vol. 12, no. 6, pp. 1223–1227, Jun. 2015.
[22] T. Celik and K.-K. Ma, "Multitemporal image change detection using undecimated discrete wavelet transform and active contours," *IEEE Trans. Geosci. Remote Sens.*, vol. 49, no. 2, pp. 706–716, Feb. 2011.
[23] J. Prendes, M. Chabert, F. Pascal, A. Giros, and J.-Y. Tourneret, "A new multivariate statistical model for change detection in images acquired by homogeneous and heterogeneous sensors," *IEEE Trans. Image Process.*, vol. 24, no. 3, pp. 799–812, Mar. 2015.
[24] Z. Wang, X. Wang, W. Wu, and G. Li, "Continuous change detection of flood extents with multisource heterogeneous satellite image time series," *IEEE Trans. Geosci. Remote Sens.*, vol. 61, 2023, Art. no. 4205418.
[25] H. Kusetogullari, A. Yavariabdi, and T. Celik, "Unsupervised change detection in multitemporal multispectral satellite images using parallel particle swarm optimization," *IEEE J. Sel. Topics Appl. Earth Observ. Remote Sens.*, vol. 8, no. 5, pp. 2151–2164, May 2015.
[26] B. Awad and I. Erer, "Unsupervised change detection in optical satellite imagery using sift flow," *Int. Arch. Photogramm., Remote Sens. Spatial Inf. Sci.*, vol. 46, pp. 47–52, Jul. 2022.
[27] B. G. Tikuye, M. Rusnak, B. R. Manjunatha, and J. Jose, "Land use and land cover change detection using the random forest approach: The case of the upper Blue Nile River Basin, Ethiopia," *Global Challenges*, vol. 7, no. 10, Sep. 2023, Art. no. 2300155.
[28] G. Mercier, G. Moser, and S. B. Serpico, "Conditional copulas for change detection in heterogeneous remote sensing images," *IEEE Trans. Geosci. Remote Sens.*, vol. 46, no. 5, pp. 1428–1441, May 2008.
[29] H. M. Alshamlan, "An effective filter method towards the performance improvement of FF-SVM algorithm," *IEEE Access*, vol. 9, pp. 140835–140840, 2021.
[30] T. Habib, J. Inglada, G. Mercier, and J. Chanussot, "Support vector reduction in SVM algorithm for abrupt change detection in remote sensing," *IEEE Geosci. Remote Sens. Lett.*, vol. 6, no. 3, pp. 606–610, Jul. 2009.
[31] N. Longbotham, F. Pacifici, T. Glenn, A. Zare, M. Volpi, D. Tuia, E. Christophe, J. Michel, J. Inglada, J. Chanussot, and Q. Du, "Multimodal change detection, application to the detection of flooded areas: Outcome of the 2009–2010 data fusion contest," *IEEE J. Sel. Topics Appl. Earth Observ. Remote Sens.*, vol. 5, no. 1, pp. 331–342, Feb. 2012.
[32] T. Hoberg, F. Rottensteiner, R. Q. Feitosa, and C. Heipke, "Conditional random fields for multitemporal and multiscale classification of optical satellite imagery," *IEEE Trans. Geosci. Remote Sens.*, vol. 53, no. 2, pp. 659–673, Feb. 2015.
[33] M. Li, X. Liu, X. Wang, and P. Xiao, "Detecting building changes using multimodal Siamese multitask networks from very-high-resolution satellite images," *IEEE Trans. Geosci. Remote Sens.*, vol. 61, 2023, Art. no. 5404322.
[34] X. Zhang, Y. Yue, W. Gao, S. Yun, Q. Su, H. Yin, and Y. Zhang, "DifUnet++: A satellite images change detection network based on Unet++ and differential pyramid," *IEEE Geosci. Remote Sens. Lett.*, vol. 19, pp. 1–5, 2022.
[35] R. Jing, Z. Gong, and H. Guan, "Land cover change detection with VHR satellite imagery based on multi-scale SLIC-CNN and SCAE features," *IEEE Access*, vol. 8, pp. 228070–228087, 2020.
[36] K. S. Basavaraju, N. Sravya, S. Lal, J. Nalini, C. S. Reddy, and F. Dell'Acqua, "UCDNet: A deep learning model for urban change detection from bi-temporal multispectral Sentinel-2 satellite images," *IEEE Trans. Geosci. Remote Sens.*, vol. 60, 2022, Art. no. 5408110.
[37] A. Chouhan, A. Sur, and D. Chutia, "DRMNet: Difference image reconstruction enhanced multiresolution network for optical change detection," *IEEE J. Sel. Topics Appl. Earth Observ. Remote Sens.*, vol. 15, pp. 4014–4026, 2022.
[38] W. Zhang, Y. Zhang, L. Su, C. Mei, and X. Lu, "Difference-enhancement triplet network for change detection in multispectral images," *IEEE Geosci. Remote Sens. Lett.*, vol. 20, pp. 1–5, 2023.
[39] F. Pacifici, F. Del Frate, C. Solimini, and W. J. Emery, "An innovative neural-net method to detect temporal changes in high-resolution optical satellite imagery," *IEEE Trans. Geosci. Remote Sens.*, vol. 45, no. 9, pp. 2940–2952, Sep. 2007.
[40] H. Sahbi, "Interactive satellite image change detection with context-aware canonical correlation analysis," *IEEE Geosci. Remote Sens. Lett.*, vol. 14, no. 5, pp. 607–611, May 2017.
[41] H. M. Alshamlan, G. H. Badr, and Y. A. Alohali, "ABC-SVM: Artificial bee colony and SVM method for microarray gene selection and multi class cancer classification," *Int. J. Mach. Learn. Comput.*, vol. 6, no. 3, pp. 184–190, Jun. 2016.
[42] [Online]. Available: http://earthexplorer.usgs.gov

BIPIN SHAH completed his secondary education from Delhi Public School Varanasi. He is currently pursuing the bachelor's degree with the Computer Science and Engineering Program, Vellore Institute of Technology. Notably, he has contributed to academic research by publishing a conference papers, showcasing his dedication to advancing knowledge in his chosen field. As, he progresses in his academic journey, he continues to explore and deepen his understanding of the intersection between computer science, artificial intelligence, and machine learning. His current research interests include artificial intelligence and machine learning.

AYUSHI GUPTA completed her 12th education from the Prof. Rajendra Singh Senior Secondary School. She is currently pursuing the bachelor's degree with the Computer Science and Engineering Program, Vellore Institute of Technology. Notably, she has contributed to academic research by publishing a conference papers, showcasing her dedication to advancing knowledge in her chosen field. As, she progresses in her academic journey, she continues to explore and deepen her understanding of the intersection between computer science, machine learning, and data analytics. Her current research interests include machine learning and data analytics.

SOURABH PAUL received the B.E. degree in electronics and telecommunication engineering from Tripura Institute of Technology, Tripura, India, in 2011, the M.Tech. degree in electronics and communication engineering from the National Institute of Technology, Agartala, India, in 2014, and the Ph.D. degree in electronics and communication engineering from the National Institute of Technology, Rourkela, India, in 2019. Currently, he is an Assistant Professor (Senior) with the School of Electronics Engineering (SENSE), Vellore Institute of Technology (VIT), Chennai. He has the working experience of nearly ten years in research and teaching field. His research interests include image registration, image matching, remote sensing image processing, and edge detection. He has authored or coauthored a number of IEEE geoscience and remote sensing letters, IEEE journals of selected topics in applied earth observations and remote sensing and other research articles on remote sensing image processing.